Interplay of chiral and helical states in a Quantum Spin Hall Insulator lateral junction

M. R. Calvo,[1,2,3,4,*] F. de Juan,[5,†] R. Ilan,[6,5] E. J. Fox,[1,2] A. J. Bestwick,[1,2] M. Mühlbauer,[7] J. Wang,[1,2,8] C. Ames,[7] P. Leubner,[7] C. Brüne,[7] S. C. Zhang,[1,2] H. Buhmann,[7] L. W. Molenkamp,[7] and D. Goldhaber-Gordon[1,2,‡]

[1]*Department of Physics, Stanford University, Stanford, California 94305, USA*
[2]*Stanford Institute for Materials and Energy Sciences, SLAC National Accelerator Laboratory, Menlo Park, California 94025, USA*
[3]*CIC nanoGUNE, 20018 Donostia-San Sebastian, Spain*
[4]*Ikerbasque, Basque Foundation for Science, 48013 Bilbao, Spain*
[5]*Department of Physics, University of California, Berkeley, California 94720, USA*
[6]*Raymond and Beverly Sackler School of Physics and Astronomy, Tel Aviv University, Tel Aviv 69978, Israel*
[7]*Physikalisches Institut (EP3) and Röntgen Center for Complex Material Systems, Universität Würzburg, Am Hubland, 97074 Würzburg, Germany*
[8]*State Key Laboratory of Surface Physics and Department of Physics, Fudan University, Shanghai 200433, China*

(Dated: March 1, 2017)

We study the electronic transport across an electrostatically-gated lateral junction in a HgTe quantum well, a canonical 2D topological insulator, with and without applied magnetic field. We control carrier density inside and outside a junction region independently and hence tune the number and nature of 1D edge modes propagating in each of those regions. Outside the 2D gap, magnetic field drives the system to the quantum Hall regime, and chiral states propagate at the edge. In this regime, we observe fractional plateaus which reflect the equilibration between 1D chiral modes across the junction. As carrier density approaches zero in the central region and at moderate fields, we observe oscillations in resistance that we attribute to Fabry-Perot interference in the helical states, enabled by the broken time reversal symmetry. At higher fields, those oscillations disappear, in agreement with the expected absence of helical states when band inversion is lifted.

arXiv:1702.08561v1 [cond-mat.mes-hall] 27 Feb 2017

Above a certain critical thickness, the 2-dimensional electron gas (2DEG) of a HgTe quantum well presents an inverted band structure characteristic of a 2D topological insulator (2D-TI) [1, 2]. At the edge of the topological insulator, quantum spin Hall (QSH) helical states propagate [3, 4]. When the Fermi level lies in the bulk gap of a 2D-TI, conduction is dominated by those edge states [5, 6] and is in principle protected by time-reversal symmetry (TRS) against single-electron backscattering processes. The application of magnetic field is expected to lift such TRS protection. Nonetheless, band inversion remains and counterpropagating QSH-like edge states are predicted to persist up to a critical magnetic field B_c. Above this field, band inversion should disappear, leaving a 2D band structure identical to that of a *topologically trivial* [7] semiconductor in the Quantum Hall (QH) regime [5, 6, 8].

Previous experiments on HgTe quantum wells in this thickness range show that the resistance in the 2D gap increases in the presence of moderate magnetic fields [6, 9, 10] as predicted [8, 11], but our understanding of the evolution of edge conduction with magnetic field is incomplete. For the related problem of assigning quantum numbers to different chiral quantum Hall (QH) modes, a fruitful approach has been to study scattering between those modes by measuring transport through junctions between regions of different carrier density This approach has been widely applied in GaAs quantum wells (for a review see Ref. [12]) and more recently in the Dirac 2DEG of graphene [13–16]. Thus, to characterize helical modes under broken TRS, studying their interplay with quantum Hall chiral states could be a promising strategy.

In this work, we explore electronic transmission across a lateral heterojunction fabricated on a HgTe quantum well with inverted band structure. Above a critical field, our results are consistent with expectations for equilibration of QH edge modes. Results are similar below the critical field for high carrier densities, but clearly differ when the junction is tuned through zero density. There, we first observe how the maximum of resistance associated with the bulk gap appears shifted towards lower values of applied gate voltage. We find this to be a consequence of the remaining band inversion. Over the density regime corresponding to the peak shift, the resistance of our device presents oscillations which we attribute to Fabry-Perot interference of helical states enabled by the lifting of TRS protection. This differs from the scenario presented in Ref. [17] for the interplay of chiral QH and helical QSH states.

Fig. 1(a) presents the geometry of our device. A Hall bar mesa is defined following the method described in Ref. [18] on a HgTe quantum well with inverted band structure. The 2DEG is formed in a quantum well epitaxially grown over a conductive substrate [19], allowing for the application of an overall back-gate voltage. Details on the layer structure and fabrication process are described in [20]. A narrow top gate electrode is placed at the center of the device, defining two regions with separately-tunable density (inset of Fig. 1(c)). *Central region* refers to the area covered by the top-gate electrode and *outer region* to its surroundings. The carrier density in the outer region n can be tuned by the ap-

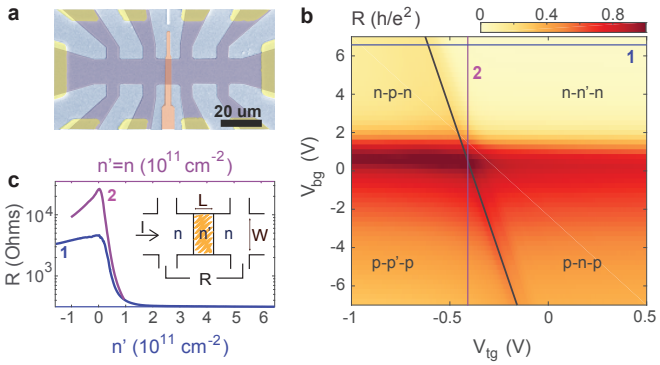

FIG. 1. (a) Electron micrograph of Hall bar device with narrow top gate. The geometry of the device is sketched in the inset of panel (c). The width (W) of the Hall bar is 10 μm and the physical length (L) of the top gate is 2 μm. Carrier density in the outer and central regions of the junction are denoted by n and n' respectively. (b) 4-terminal resistance (R) across top-gated region measured as sketched in the inset of panel (c) as a function of top gate and back gate voltages at zero applied magnetic field. The diagonal black line marks the estimated position of $n' = 0$. (c) Selected linecuts extracted from panel (b): Linecut 1 (blue) shows the evolution of R as a function only of $V_{\rm tg}$, that is, along with n' while the outer region is kept at constant $n = 10^{11}$ cm^{-2}. Linecut 2 shows R as function solely of $V_{\rm bg}$, which changes the density of the whole device, for a value of $V_{\rm tg} = V_{\rm tg0}$ such that the device density is homogeneous, that is, $n' \simeq n$.

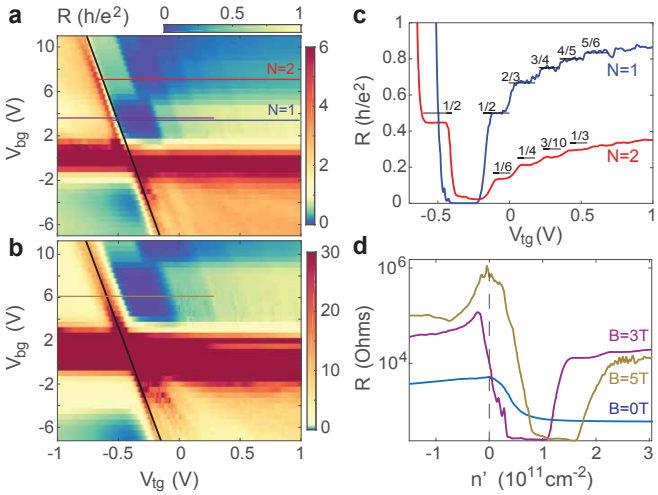

FIG. 2. (a),(b) 2D maps of resistance obtained at B = 3 and 5 T respectively. The color scale has been chosen to enhance the contrast in the $n - n' - n$ region between 0 and 1 h/e^2. The fractional resistance values match predictions for electron transmission from N QH edge modes in the outer regions of the junction into N' modes in the central region *in the presence of edge mode equilibration*. (c) Horizontal linecuts from panel (a), at $V_{\rm bg} = 3.5$ V (blue) and 7 V (red), corresponding to $N = 1$ and $N = 2$. N' is tuned by the top-gate voltage $V_{\rm tg}$. (d) Four-terminal resistance R as a function of density in the junction for $B = 0$ (blue), $B = 3$ (magenta), $B = 5$ T (yellow) for density in the outer region $n = 5 \times 10^{10}$, 5×10^{10}, 8×10^{10} cm^{-2} respectively. For the cases with finite applied field, those carrier densities correspond to $N = 1$.

plied back-gate voltage V_{bg}, while n' depends on both back- and top-gate (V_{tg}) voltages. Both n and n' can be estimated using a simple capacitor model [20].

Fig. 1(b) shows the evolution of the four-terminal resistance R measured across the junction at 2.1 K (inset of Fig. 1(c)) as a function of both V_{bg} and V_{tg} at zero applied magnetic field. As previously reported, the resistance presents a finite maximum when the chemical potential lies in the bulk gap and conduction is dominated by the QSH edge states. As a function of spatially-uniform carrier density, four-terminal resistance (Curve 2 in Fig. 1(c)) shows a maximum value higher than $h/2e^2$, the value associated with the ballistic Quantum Spin Hall regime. This is expected: the edge mean free path in similar heterostructures has been reported to be a few microns [5], substantially less than the edge length between contacts in the present geometry, so backscattering should result in increased resistance. In contrast, as a function only of density in the junction (Curve 1 in Fig. 1(c)) the maximum resistance is lower than $h/2e^2$, suggesting the presence of bulk conduction in parallel to the QSH edge states. A detailed look at the data (Fig. S2 of [20]) reveals oscillations in the resistance which likely arise from the constructive interference of those bulk non-localized states (for a detailed analysis see [20]).

The locations of resistance maxima in the $(V_{\rm tg}, V_{\rm bg})$ parameter space (Fig. 1(a)) fall along two lines: a horizontal line around $V_{\rm bg} = V_{\rm bg0} = 0$ V representing zero density in the outer region, and a diagonal line representing zero density in the central region of the junction ($n' = 0$):

$$(V_{\rm tg} - V_{\rm tg0}) = -(C_{\rm bg}/C_{\rm tg})(V_{\rm bg} - V_{\rm bg0}). \qquad (1)$$

A fit to this diagonal line (black, Fig. 1(b)) yields the ratio between top and back-gate capacitance $C_{\rm tg}/C_{\rm bg}$. The two lines define four quadrants of electron and hole densities in the central and outer regions of the junction, labeled in Fig. 1(b).

Small Fabry-Perot oscillations appear in the resistance at the bipolar quadrants (see Fig. S2 in [20]), with similar behavior to other 2DEG junctions [21, 22]. The period of the oscillations suggests that the electrostatic profile of our junction is shorter than its actual physical length: our analysis yields an effective length $L^* = 0.6 \pm 0.1$ μm (for a detailed analysis see [20]).

At finite fields, four-terminal resistance R in the n-n'-n quadrant shows a sharp tiled pattern of fractional resistance values ranging from 0 to h/e^2 (Fig. 2(a,b), $B = 3$ and 5 T respectively.) The Landauer-Büttiker formalism describes those fractional values as the result of full equilibration between co-propagating edge states in the junction (cf. [12, 14, 23].) In the unipolar regime and in a 4-terminal configuration, the predicted resistance across

the junction is given by

$$R = \frac{h}{e^2}\frac{N - N'}{NN'} \quad (2)$$

where N and N' are the number of quantum Hall states propagating in the outer and central regions of the junction respectively. The bottom row of tiles in Fig. 2(a,b) corresponds to $N = 1$, with N' increasing from left to right. Our data show a good agreement with the fractional plateaus at $R = 0, 1/2, 2/3, 3/4, ...$ expected for $N' = 1, 2, 3, 4, ...$ ($N = 1$ linecut in Fig. 2(c)). Similarly, a second row of tiles appears for $N = 2$, and in the corresponding linecut of Fig. 2(a), plateaus of resistance can be observed near the expected values for $N = 2$ paired with a range of N', although deviations from the ideal behavior are larger here than for $N = 1$. Similarly, plateaus are observed near but not exactly at the expected values for the p-p'-p and the n-p-n quadrants (see [20] for details.)

These results highlight the role of the strong spin-orbit interaction in HgTe. In absence of spin-orbit interaction, spin is a good quantum number. Transmission would then be spin-selective and only those states with same spin polarization would equilibrate, leading to fewer plateaus in resistance R. In contrast, our data suggest that full equilibration occurs for all possible values of N and N': the strong spin-orbit coupling of HgTe allows edge states with different spin orientations to mix [24].

The tiled structure of fractional resistance values in the n-n'-n quartet is similar at both 3 and 5 T (Fig. 2(a) and (b) respectively), the only difference being the range of densities at which each resistance tile, associated to a given pair of values (N,N'), is reached. In contrast, a different behavior emerges around zero density. First, the zero density $n' = 0$ line (Eq. 1) determined from zero magnetic field data in Fig. 1(b) is overlaid for reference on Fig. 2(a) and (b). The maximum of resistance at $B = 3$ T is clearly shifted towards lower values of V_{tg} with respect to that line. Remarkably, it returns to the original position at $B = 5$ T (Fig. 2(b)). This effect can be also observed in the horizontal linecuts taken from the corresponding 2D resistance plots at similar outer densities n for 0, 3 and 5 T (Fig. 2(d)). Furthermore, this plot reveals strong oscillations in the resistance near zero density at 3 T, coincidentally with the shift of the resistance peak.

To further understand these results, we present calculations of band structure below and above the critical field, (details in [20]) for the magnetic fields considered in the experiment, $B = 0, 3, 5$ T (Fig. 3(a)). At zero field, when the Fermi energy lies in the bulk gap, we find the usual counterpropagating helical edge states. At both $B = 3$ and 5 T conduction and valence bands turn into a set of discrete Landau levels (LLs). When the Fermi level lies in the gap between LLs, one chiral Quantum Hall state propagates at the edge for each filled Landau

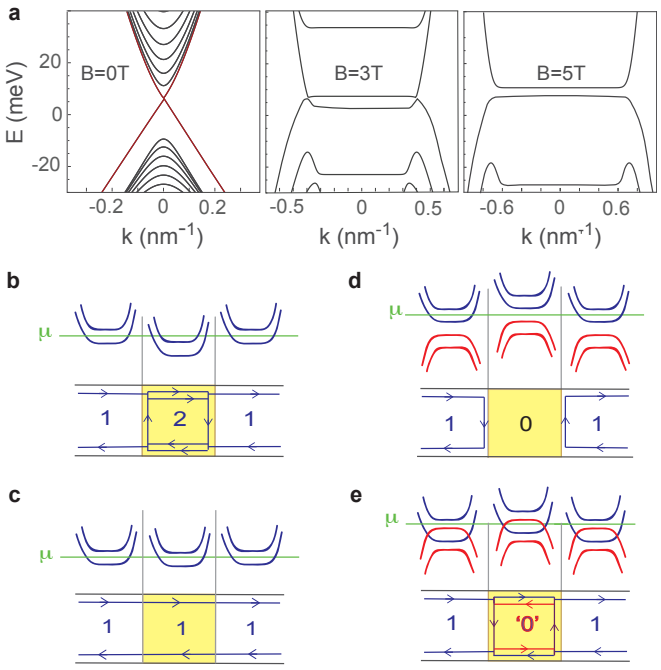

FIG. 3. (a) Computed band structure of a strained 7.5 nm HgTe quantum well at 0, 3 and 5 T. The critical field $B_c = 3.8$ T in the model. See [20] for calculation details. (b),(c) Sketch of band structure and edge states in different scenarios at 3 and 5 T where the outer region hosts one chiral edge state and the inner region hosts either two or one, respectively. (d),(e) Similar sketches for the case $N = 1$ and $N' = 0$ for 5 and 3 T. (d) Above B_c a broad gap opens between the electron and hole Landau levels so no states propagate at the junction. (e) Below B_c, band inversion remains and at $\nu = 0$ a helical mode propagates in the junction.

level in the bulk and the total number of modes N is given by the integer part of the filling factor ν. For fields $B < B_c$ such as $B = 3$ T, the lowest order hole-like and electron-like Landau levels are inverted in the bulk and cross near the edge, so when the Fermi level is in the bulk gap there are counterpropagating edge states (we further refer to this regime as $\nu = 0$). By 5 T, which is above B_c, the band inversion has disappeared, and the material resembles a *trivial* semiconductor, with a gap between electron and hole Landau levels.

In the junction geometry considered in our experiment, the chemical potential in the central and outer regions can be tuned independently. At finite field, the electronic transmission across the device will thus result from the matching of edge modes corresponding to different fillings at both the central and outer regions of the junction (ν' and ν respectively).

When the central region has $\nu' \neq 0$, the edge mode structure is the usual one observed in quantum Hall experiments with standard 2DEGs, (see for example the cases N-N'-N = 1-2-1 and 1-1-1 sketched in Figs. 3(b,c)). As explained above, the resulting resistance in this case

is given by a Landauer-Büttiker expression (Eq. 2) assuming full equilibration of co-propagating edge modes, and the match to our data is quite good. When $\nu' = 0$ however, the situation changes drastically depending on whether B is larger or smaller than B_c. Above the critical field, the Fermi level always lies in a bulk gap with no edge modes, and incoming modes are always reflected, as illustrated in Fig. 3(d) for the case 1-0-1. Below the critical field, in contrast, the band inversion requires the presence in the inner region of two QSH-like edge states with opposite chiralities (Fig. 3(e)). Edge modes cannot simply terminate, so a mode must also propagate along the 1-0 and 0-1 interfaces.

We believe that the matching of chiral to helical edge states in the 1-0-1 scenario is the origin of the resistance oscillations and the shift in the position of the resistance maximum we observe at 3 T (Fig. 2(d)). To understand this, we first note that since TRS is broken at finite field, the crossing of QSH edge modes when $B < B_c$ is only protected in the presence of extra symmetries such as mirror. In the experimentally relevant case, there should always be a small minigap (induced for example by bulk inversion asymmetry, and in general dependent on the junction details) with the crossing becoming an anticrossing (Figs. 4a-c). The location of this anticrossing within the gap depends on details such as the potential at the edge, so the resistance maximum originating from the minigap will be in general shifted with respect to the one induced by a bulk gap. The observed maximum being shifted and significantly narrower at 3 T than at zero or 5 T (see Fig. 2(d)) is consistent with having its origin in the edge state mini-gap.

Further support for the presence of the helical edge modes comes from the observed oscillations. To understand this, we focus on the edge mode structure in more detail, following Figs. 4(a-c). In the 1-0-1 configuration, when the incoming chiral edge mode from the outer region reaches the junction, it can scatter into two possible outgoing modes: the co-propagating helical edge mode or the chiral mode parallel to the junction. When the chemical potential in the central region is very near the bottom of the first Landau Level the incoming edge mode is almost perfectly matched to the copropagating helical one, while the counterpropagating edge mode forms a loop spanning the whole junction (Fig. 4(a)). This must be so because the counterpropagating mode has smaller momentum and therefore is located further from the edge. Transport in this scenario is almost equivalent to the 1-1-1 situation, seen in the experimental data as an extension of the $R = 0$ plateau to lower densities (Fig. 2(a)).

As the chemical potential gets near the crossing of the helical edge modes, the chiral mode connects to the one parallel to the junction, while the helical modes form a loop at either edge (Fig. 4(b)).These loops should disappear at the minigap, and reappear with opposite orientation below it (Fig. 4(c)). The existence of these loops, allowed because the protection from backscattering is lifted by B, implies that coherent transport should be affected by multiple reflections at the interfaces. This effect should be manifest in Fabry-Perot type oscillations as a function of chemical potential, because the accumulated phase $\delta = kL$ will also change. This explains the zero-density oscillations observed at 3 T in Fig. 2, their occurrence in the density range assigned to the bulk gap, and their disappearance beyond B_c (i.e. at 5 T) where no helical modes exist.

Fig. 4(d) shows the evolution of the oscillations as a function of the 2D-densities in the central and outer regions, n' and n respectively, where a smoothed resistance background has been removed for clarity (for details see [20]). Oscillations are periodic in n', with no substantial dependence on n. This is consistent with our interpretation: changing n' will change the edge momentum of the loop modes and hence the phase, while n only determines the momentum of the incoming modes, which should have no effect on the phase of the oscillations. Fig. 4(d) also shows that oscillations are present for n values corresponding to N=1, but they disappear when approaching $N = 2$. This is consistent with the N=2 Quantum Hall chiral edge modes not being fully established at $B = 3$ T, as already seen in the imperfectly-quantized equilibration plateaus in Fig. 2(c).

Finally, assuming a Fabry-Perot scenario yields an estimate of the 1D edge mode carrier density (n_{1D}). Whereas the 2D carrier density (n) can be easily estimated by means of a simple capacitor model (see [20]), estimating how the gate voltage changes n_{1D} is not trivial. In a simple approximation and for a particle-in-the-box model, in one dimension, one would expect the period of Fabry-Perot oscillations to be constant and given by $\delta(n_{1D}) = g/L$, where g is the state degeneracy and L the length of the junction. Assuming $g = 2$, $L = 0.6$ μm, and $\delta(V_{tg}) \simeq 0.024$ V being the resistance oscillation voltage period of our data, we infer a one-dimensional capacitance for the edge mode of $C_{1D} = \delta(n_{1D})/\delta(V_{tg}) \simeq 1.4 \times 10^6$ cm^{-1}V^{-1}. Here, it should be noted that the presence of a few impurities in an otherwise ballistic edge can also give rise to oscillations with a length scale that is different to the actual junction length [11], thus modifying this estimate.

Our results below critical field are compatible with those in Ref. [17], where the observation of finite resistance at $\nu' = 0$ implies that counterpropagating states remain in this regime. The shorter length of our junction (0.6 compared to 3 μm) allows for the observation of coherent interference, which was not seen in that work. Besides, we also explore here the transition between QSH and QH regimes at the junction which is not reached in the work by Gusev et al. [17].

In conclusion, we have characterized a lateral junction on a HgTe quantum well with inverted band structure. Under applied field we observe sharp fractional plateaus

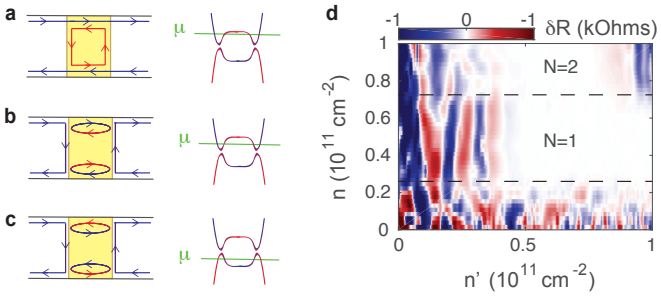

FIG. 4. (a),(b),(c) Possible scenarios for edge state matching in the 1-0-1 situation. (d) Zoom in the δR oscillations as a function of 2D density in the central and outer regions of the junction, n, n', at applied field $B = 3$ T. Areas with different numbers of quantum hall modes ($N = 1$ and $N = 2$), i.e. integer filling factor, in the outer region are separated by dotted lines.

in the resistance at high electron densities. Their values agree with Landauer-Büttiker predictions based on full equilibration of co-propagating edge states even for opposite spins, presumably because of strong spin-orbit coupling. Below the critical field for band inversion, we found features in the resistance that can be associated with the presence of counterpropagating helical edge states when the central region is at low density. These features include a shift in the gate voltage at which resistance is maximized, and Fabry-Perot type oscillations induced by backscattering at the edges of the central region. Above the critical field, those oscillations disappear, in agreement with the expected absence of helical states when band inversion is lifted. While further studies are necessary for full characterization, our results suggest that valuable information about the QSH state under broken TRS can be inferred from the electronic transmission across a QH-QSH-QH heterojunction.

The work at Stanford was supported by Department of Energy, Office of Basic Energy Sciences, Division of Materials Sciences and Engineering, under contract DE-AC02-76SF00515 to D.G.-G. and S.-C.Z. The Center for Probing the Nanoscale, an NSF NSEC under grant PHY-0830228 to D.G.-G. supported early stages of the project. The European Union under the project FP7-PEOPLE-2010-274769 supported M.R.C.'s stay at Stanford. We also acknowledge support from the National Thousand-Young-Talents Program to J.W. and funding from an AFOSR MURI (F.J.) and from the DARPA FENA program (R.I.). The Würzburg group acknowledges additional financial support from the German Research Foundation (The Leibniz Program, Sonderforschungsbereich 1170 Tocotronics and Schwerpunktprogramm 1666), the EU ERC-AG program (Project 3-TOP), the Elitenetzwerk Bayern IDK Topologische Isolatoren and the Helmoltz Foundation (VITI).

* E-mail: rcalvo@nanogune.eu or mreyescalvo@gmail.com
† Present address:Rudolf Peierls Centre for Theoretical Physics, Oxford University, UK
‡ E-mail: goldhaber-gordon@stanford.edu

[1] X.-L. Qi and S.-C. Zhang, Reviews of Modern Physics **83**, 1057 (2011).
[2] M. Z. Hasan and C. L. Kane, Reviews of Modern Physics **82**, 3045 (2010).
[3] C. L. Kane and E. J. Mele, Physical review letters **95**, 226801 (2005).
[4] B. A. Bernevig, T. L. Hughes, and S.-C. Zhang, Science **314**, 1757 (2006).
[5] M. König, S. Wiedmann, C. Brüne, A. Roth, H. Buhmann, L. W. Molenkamp, X.-L. Qi, and S.-C. Zhang, Science **318**, 766 (2007).
[6] M. König, H. Buhmann, L. W. Molenkamp, T. Hughes, C.-X. Liu, X.-L. Qi, and S.-C. Zhang, Journal of the Physical Society of Japan **77**, 031007 (2008).
[7] The electronic structure of a 2DEG in the Quantum Hall regime is also topologically nontrivial. Here, however, we use trivial to describe only the lowest energy bands characterized by the Z2 topological invariant.
[8] B. Scharf, A. Matos-Abiague, and J. Fabian, Physical Review B **86**, 075418 (2012).
[9] G. Gusev, E. Olshanetsky, Z. Kvon, N. Mikhailov, and S. Dvoretsky, Physical Review B **87**, 081311 (2013).
[10] J. Maciejko, X.-L. Qi, and S.-C. Zhang, Physical Review B **82**, 155310 (2010).
[11] G. Tkachov and E. M. Hankiewicz, Physical review letters **104**, 166803 (2010).
[12] R. Haug, Semiconductor science and technology **8**, 131 (1993).
[13] J. Williams, L. DiCarlo, and C. Marcus, Science **317**, 638 (2007).
[14] B. Özyilmaz, P. Jarillo-Herrero, D. Efetov, D. A. Abanin, L. S. Levitov, and P. Kim, Physical review letters **99**, 166804 (2007).
[15] D.-K. Ki and H.-J. Lee, Physical Review B **79**, 195327 (2009).
[16] F. Amet, J. Williams, K. Watanabe, T. Taniguchi, and D. Goldhaber-Gordon, Physical review letters **112**, 196601 (2014).
[17] G. Gusev, A. Levin, Z. Kvon, N. Mikhailov, and S. Dvoretsky, Physical review letters **110**, 076805 (2013).
[18] E. Y. Ma, M. R. Calvo, J. Wang, B. Lian, M. Mühlbauer, C. Brüne, Y.-T. Cui, K. Lai, W. Kundhikanjana, Y. Yang, *et al.*, Nature communications **6** (2015).
[19] P. Leubner, L. Lunczer, C. Brüne, H. Buhmann, and L. W. Molenkamp, Physical Review Letters **117** (2016), 10.1103/physrevlett.117.086403.
[20] See Supplemental Material at [URL will be inserted by publisher].
[21] A. F. Young and P. Kim, Nature Physics **5**, 222 (2009).
[22] A. Varlet, M.-H. Liu, V. Krueckl, D. Bischoff, P. Simonet, K. Watanabe, T. Taniguchi, K. Richter, K. Ensslin, and T. Ihn, Phys. Rev. Lett. **113**, 116601 (2014).
[23] J. R. Williams, D. A. Abanin, L. DiCarlo, L. S. Levitov, and C. M. Marcus, Physical Review B **80**, 045408 (2009).
[24] G. Müller, D. Weiss, A. Khaetskii, K. Von Klitzing, S. Koch, H. Nickel, W. Schlapp, and R. Lösch, Physical Review B **45**, 3932 (1992).